Journal of
Mechanics of Materials and Structures

SHAPE OPTIMIZATION OF A RIGID INCLUSION IN A SHEAR-LOADED ELASTIC PLANE

Shmuel Vigdergauz

Volume 2, Nº 2 *February 2007*

mathematical sciences publishers

JOURNAL OF MECHANICS OF MATERIALS AND STRUCTURES
Vol. 2, No. 2, 2007

SHAPE OPTIMIZATION OF A RIGID INCLUSION IN A SHEAR-LOADED ELASTIC PLANE

SHMUEL VIGDERGAUZ

A rigid inclusion perfectly embedded in a thin plate is considered as a two-dimensional elastostatic composite structure to solve the inverse problem of finding the inclusion shape around which the local maximum of the von Mises equivalent stresses attain the global minimum under shear loading at infinity. Absent optimality preconditions such as the equistress principle for bulk-type loading, a fast and accurate assessment of a given shape is developed by combining complex-valued series expansions with a new infinite summation scheme. This approach to solving the direct problem is then included into a genetic algorithm optimization over the set of shapes obtained from a circle by a finite-term conformal mapping with square symmetry. Compared to a circular inclusion, the stresses may thus be lowered by 15–25%, depending on the Poisson's ratio of the plate. The numerical results presented allow us to conjecture that the von Mises stresses around the optimal shape are *uniform*. The inclusion that minimizes the induced energy increment is also identified by the same approach. Both shapes appear to be very similar, though not identical.

1. Introduction

Grained and fibre-reinforced composites find broad use as construction elements. For this reason, their mechanical behavior is the subject of extensive study in elasticity. Such two-phase structures are idealized here as an infinite zero-thickness plate with perfectly bonded foreign inclusions, which may represent either a two-dimensional grain or the cross-section of a long cylindrical fibre. These mathematically equivalent cases are known as *plane stress* and *plane strain*, respectively [Muskhelishvili 1975].

We further simplify the model by assuming that the inclusions are remote from each other, so that one may neglect their interaction and consider a single inclusion in an unbounded matrix under a homogeneous elastic field σ_{xx}^{∞}, σ_{yy}^{∞}, $\sigma_{xy} = 0$ at infinity.

At finite distances, this field is distorted by the inclusion. With the layout above, the resulting stresses depend only on the inclusion geometry. This brings us to the optimization problem of finding the inclusion shape that minimizes a certain criterion. Two practically important criteria are commonly used in shape optimization: the inclusion-induced strain energy increment δW divided by the inclusion area, and the maximum $\mathcal{M}$ of von Mises equivalent stresses σ_M [Cherepanov 1997] along the material interface. On a free-traction hole, σ_M coincide with the hoop stresses, but on a rigid or elastic inclusion they involve bilinearly all the boundary stresses which, in a general way, should differ from zero to ensure the assumed perfect contact between the phases.

The exact formulation of the problem reads:

Keywords: plane elasticity problem, Kolosov–Muskhelishvili potentials, shape optimization, effective energy, extremal elastic structures, genetic algorithm.

Given the topology of the single inclusion in the matrix, the uniform static far loading and the elastic properties of the matrix, find, among all continuous curves, the rigid inclusion shape that minimizes either of the two above-mentioned criteria.

Beginning with the pioneering work of Cherepanov [1974], it was realized that the sign of the ratio $\beta = \sigma_{yy}^{\infty}/\sigma_{xx}^{\infty}$ is the main factor driving the complexity of this shape optimization problem. As applied to rigid inclusions, two basic cases are of particular interest:

• *The far loading is hydrostatic tension or compression* ($\beta = 1$). Here, attention is focused on the equistress contours [Cherepanov 1974; Vigdergauz 1976; Grabovsky and Kohn 1994], at which matrix-side boundary tractions reduce to uniform normal stresses. Remarkably, these contours not only exist for a variety of geometries but also provide the global minima for both criteria simultaneously. The single equistress inclusion is simply a circle. For interacting inclusions the equistress condition is used as a prerequisite to find their shapes by analytical or numerical solving of the coupled Dirichlet problem; see, for instance, [Grabovsky and Kohn 1994]. In other words, the optima are found without touching the direct problem of solving the stress field around any given inclusion.

• *The far load is that of pure shear* ($\beta = -1$). In this context, neither δW- nor $\mathcal{M}$-optimal shapes are known so far, because the equistress principle is no longer valid and no other optimal precondition has yet been developed instead. For this reason, the more effective strategy is the standard numerical one, where a search space of admissible shapes is first defined through a finite number of parameters, which are then optimized by repetitively solving the criterion function over many curves.

As parameters, we choose the first N Laurent coefficients d_k, $k = \overline{1, N}$, $d_k = 0$, $k > N$ of the conformal map from the exterior of the unit circle to the exterior of a given inclusion. The adoption of these coefficients not only allows the use the whole machinery of complex variable theory, but they are also naturally ordered, in the sense that the higher the coefficient, the less its global impact on the inclusion shape. Owing to this, the finite-term mapping approach of [Muskhelishvili 1975], or its revised version (see [Kalandia 1975]), performs well in the numerical treatment of the direct problem, as demonstrated in the classical book by Savin [1961] and more recently in [Jasiuk 1995].

However, such solving of the local stresses involves sums of Fourier series that are actually infinite at any N, and hence may imply an unacceptably large N to attain a reasonable accuracy in optimization practice. The finite differences scheme proposed by us in the similar context of hole shape optimization [Vigdergauz 2006] overcomes this drawback by computing the infinite sums involved *exactly*, as rational functions of $\{d_k\}$, $k \le N$. This can be done with the proviso that the first N items of the sums are solved from the $N \times N$ system of linear algebraic equations expressing the matrix-inclusion contact conditions. In fact, just this novelty makes the considered optimization problem numerically tractable. A further computational saving can be achieved due to an assumed rotational symmetry of the inclusion by which the set $\{d_k\}$ partially vanishes. For the most part, we treat here the case of square symmetry, which appears to provide the best optimal response like for a shear-loaded plate with a hole [Vigdergauz 2006].

After all these considerations, the problem to be solved is a moderate-size problem of minimizing a rational function of the arguments d_k, $k = \overline{1, N}$, subject to the two-side inequalities of mapping uniqueness [Schinzinger and Laura 1991]. This nonlinear optimization problem with linear constraints is nevertheless a computationally expensive task, which is solved by a genetic algorithm (GA), an optimization

method imitating adaptive schemes found in nature (see [Gen and Cheng 1997; Osyczka 2001] and references therein). GAs have a twofold benefit over gradient-based schemes: the latter find a local optimum, while a GA is a global optimization algorithm; and no differentiation with respect to the optimized parameters is needed at any stage.

The main results so obtained show that the δW- and $\mathcal{M}$-optimal square symmetric rigid inclusions are almost the same except for a hardly compressible or incompressible matrix material, and that their shape is close to a slightly rounded square rotated by 45 degrees with respect to the main stresses $\sigma_{xx}^{\infty}, \sigma_{yy}^{\infty}$.

The paper is structured as follows. Section 2 covers some basics of conformal mapping in two-dimensional elasticity, together with new algebraic identities derived for later use. Section 3 describes the summation scheme for the boundary stresses in the direct problem which is the basis for further considerations. After these lengthy preliminaries, the reformulated optimization problem is rather straightforward and simple. First, the one-term mapping approximation is derived analytically (Section 4) to obtain qualitative properties of the solution. The multiterm approximations are next found by the standard GA briefly described in Section 5. Numerical results are displayed and discussed in Section 6. Finally, conclusions and proposed extensions of the work can be found in Section 7.

2. Complex variable technique in plane elastostatics

2.1. ***The local stress-strain relations.*** Consider the setup in Figure 1. Let an infinite elastic plane E be strengthened by a perfectly bonded rigid inclusion with a piecewise smooth boundary Γ enclosing the origin of the Cartesian system xOy. The curve Γ divides the plane into the inclusion region S_1, of finite area f_1, and the unbounded region $S_2 = E \setminus S_1$, filled with a linearly elastic phase. Let the plane be

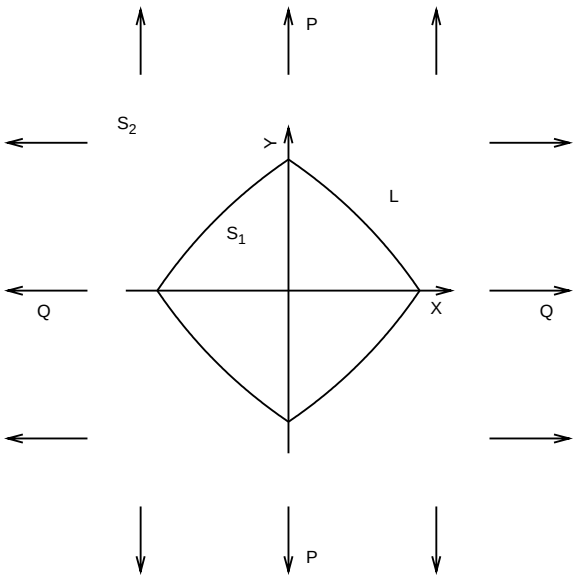

Figure 1. The problem schematic: an infinite plate with a perfectly bonded inclusion under uniform stresses, the cases $P = Q$ and $P = -Q$ correspond to remote bulk and shear, respectively. The piecewise smooth inclusion boundary possesses a certain rotational symmetry and may have a finite number of angular points.

remotely loaded by uniform nontangential stresses

$$\sigma_{xx}^{\infty} = P, \quad \sigma_{yy}^{\infty} = Q, \quad \sigma_{xy}^{\infty} = 0. \tag{1}$$

The load-induced stresses in S_2 are governed by the biharmonic Airy function which, though useful as a theoretical tool, becomes ineffective in computing local displacements. Far more advantageous is the complex variable approach of replacing the Airy function with a pair of holomorphic functions (the KM potentials; see [England 1971; Muskhelishvili 1975, §§47–51]) linked along the material interface through the contact conditions. The resulting boundary value problem is then solved using complex variable techniques. For holes and rigid inclusions the boundary conditions are further simplified by use of a conformal mapping $z = \omega(\zeta)$ from the connected matrix domain S_2 to the exterior Σ_2 of a unit circle γ. The reason is that the following identities hold on γ, in contrast to any other shape:

$$\overline{\xi} = \xi^{-1}, \qquad \int_{\gamma} \overline{\xi}^m \xi^n d\xi = \int_{\gamma} \xi^{n-m} d\xi = 2\pi i \delta_{m-n,1}, \qquad \xi \in \gamma, \tag{2}$$

where $\delta_{i,j}$ is the Kronecker delta. The mutual orthogonality of (2) makes the stress-strain computations much easier.

The KM potentials $\Phi(\zeta)$, $\Psi(\zeta)$ present the transformed stresses in $\Sigma_2 + \gamma$ as [Muskhelishvili 1975]

$$\sigma_{\rho\rho}(\zeta) + \sigma_{\theta\theta}(\zeta) = 4 \operatorname{Re} \Phi(\zeta), \qquad \zeta = \rho \exp(i\theta) : \zeta \in \Sigma_2 + \gamma, \rho \geq 1, \tag{3a}$$

$$\sigma_{\rho\rho}(\zeta) - i\sigma_{r\theta}(\zeta) = 2 \operatorname{Re} \Phi(\zeta) - \frac{\zeta^2}{\rho^2 \overline{\omega'(\zeta)}} \big(\overline{\omega(\zeta)} \Phi'(\zeta) + \omega'(\zeta) \Psi(\zeta) \big). \tag{3b}$$

The zero-displacement condition at the rigid interface γ is [Muskhelishvili 1975]

$$\lambda \overline{\varphi(\xi)} - \overline{\omega(\xi)} \frac{\varphi'(\xi)}{\omega'(\xi)} - \psi(\xi) = 0; \qquad \xi \in \gamma, \tag{4}$$

$$\lambda = \frac{3 - \nu_{\text{stress}}}{1 + \nu_{\text{stress}}}, \qquad \nu_{\text{stress}} \in [0; 1] \qquad \text{for plane stress}, \tag{5a}$$

$$\lambda = 3 - 4\nu_{\text{strain}}, \qquad \nu_{\text{strain}} = \frac{\nu_{\text{stress}}}{1 + \nu_{\text{stress}}} \in [0.5; 1] \qquad \text{for plane strain}, \tag{5b}$$

where

$$\varphi'(\zeta) \equiv \Phi(\zeta)\omega'(\zeta), \qquad \psi'(\zeta) \equiv \Psi(\zeta)\omega'(\zeta). \tag{6}$$

To save room, nonobservable negative values of ν will be excluded from the numerical simulations (Section 6). Then, both cases form the same interval $1 \leq \lambda \leq 3$ for λ, which thus serves as a unified elastic parameter of the problem. The minimum value $\lambda = 1$ corresponds to a rigid inclusion in a soft incompressible matrix.

Finally, integration of (3b) with the multiplier $\overline{\xi^2 \omega'(\xi)}\, d\xi$ along γ results in the boundary stress condition [Muskhelishvili 1975] structurally similar to (4):

$$\overline{\varphi(\xi)} + \overline{\omega(\xi)} \frac{\varphi'(\xi)}{\omega'(\xi)} + \psi(\xi) = f(\xi), \qquad \xi \in \gamma, \tag{7}$$

where the tractions $f(\xi)$ take the form

$$f(\xi) = \int_\gamma \big(\sigma_{\rho\rho}(\xi) - i\sigma_{r\theta}(\xi)\big)\,\overline{\xi^2\omega'(\xi)}\,d\xi. \tag{8}$$

2.2. ***One-potential formulation of the forward rigid inclusion problem.*** The homogeneous boundary condition (4) allows us to derive new relations which, though simple, have not, to our knowledge, been noticed in the literature so far. They give the stress components along γ through only one rather than both KM potentials, and are crucial for further analysis. To this end, we combine (4) and (7) to obtain

$$(\lambda+1)\overline{\phi(\xi)} = f(\xi), \qquad \xi \in \gamma. \tag{9}$$

Differentiating (9) in view of Equations (3a), (6), (8) yields for the real and imaginary parts of $\Phi(\xi)$

$$\sigma_{\rho\rho}(\xi) = (\lambda+1)\,\mathrm{Re}\,\Phi(\xi), \quad \sigma_{\theta\theta}(\xi) = (3-\lambda)\,\mathrm{Re}\,\Phi(\xi), \quad \sigma_{\rho\theta}(\xi) = (\lambda+1)\,\mathrm{Im}\,\Phi(\xi), \quad \xi \in \gamma. \tag{10}$$

At $\lambda = -1$ (the Dundurs correspondence, [Jasiuk 1995]), the identities in (10) formally turn into the traction-free conditions along a hole:

$$\sigma_{\rho\rho}(\xi), \sigma_{\rho\theta}(\xi) = 0, \quad \sigma_{\theta\theta}(\xi) = 4\,\mathrm{Re}\,\Phi(\xi), \tag{11}$$

or, equivalently, in KM terms, the homogeneous condition (7)

$$\overline{\varphi(\xi)} + \overline{\omega(\xi)}\,\frac{\varphi'(\xi)}{\omega'(\xi)} + \psi(\xi) = 0, \quad \xi \in \gamma, \tag{12}$$

explicitly repeated here for future reference. Namely the resemblance of the zero-traction and the zero-displacements boundary conditions (12), (4) leads to the resolving relations (10).

Except in these two homogeneous cases, the computation of boundary stresses does involve the second potential $\Psi(\xi)$, which presents additional difficulties.

In this context, a disadvantage of the mapping technique is that it returns the local stresses (10) from Σ_2 to the physical domain S_2 only as two invariant combinations I_1, I_2 rather than separately [Muskhelishvili 1975]:

$$I_1(\zeta) = \sigma_{\rho\rho}(\zeta) + \sigma_{\theta\theta}(\zeta) = I_1(z) = \sigma_{rr}(z) + \sigma_{tt}(z), \tag{13a}$$

$$I_2(\zeta) = \sigma_{\rho\theta}^2 - \sigma_{\rho\rho}(z)\sigma_{\theta\theta}(z) = I_2(z) = \sigma_{r\vartheta}^2 - \sigma_{rr}(z)\sigma_{\vartheta\vartheta}(z), \tag{13b}$$

$$z = \omega(\zeta) = r\exp(i\vartheta).$$

However, this is sufficient for our purpose of minimizing the von Mises equivalent stresses $\sigma_M(\zeta)$ along Γ:

$$\sigma_M^2(z) = \sigma_M^2(\zeta) = I_1^2(\zeta) + 3I_2(\zeta), \qquad \zeta \in \Sigma_2 + \gamma, \quad z = \omega(\zeta) \in S_2 + \Gamma. \tag{14}$$

Through the use of (13), we can express the stresses in terms of $\Phi(\xi)$ ($\xi = \exp i\theta \in \gamma$, $t = \omega(\xi) \in \Gamma$):

$$\sigma_M^2(t) = D_1(\lambda)\,\mathrm{Re}^2\,\Phi(\xi) + D_2(\lambda)\,\mathrm{Im}^2\,\Phi(\xi), \qquad D_1(\lambda) = 7 - 6\lambda + 3\lambda^2, \quad D_2(\lambda) = 3(1+\lambda)^2, \tag{15a}$$

$$\mathcal{M} \equiv \max_{t\in\Gamma} |\sigma_M(t)| = \max_{0\le\theta\le 2\pi} |\sigma_M(\theta)|. \tag{15b}$$

Further, the boundary value function $\Psi(\xi)$ is routinely eliminated from the homogeneous condition (9) by integrating over γ with the kernel $(\xi-\eta)^{-1}$, $\xi, \eta \in \gamma$ [Muskhelishvili 1975]. This leads to a Cauchy-type singular integral equation in $\Phi(\xi)$:

$$\frac{1}{2}F(\eta)+\frac{1}{2\pi i}\int_{\gamma}\frac{F(\xi)}{\eta-\xi}d\xi=(1-\lambda)\Phi(\infty)+\Psi(\infty), \tag{16a}$$

$$F(\xi)\equiv 2\overline{\xi^2\omega'(\xi)}\,\mathrm{Re}\,\Phi(\xi)-\overline{\omega(\xi)}\Phi'(\xi), \quad \xi,\eta\in\gamma, \tag{16b}$$

where the function's asymptotic behavior is dictated by the applied loads (1) (see [Muskhelishvili 1975]):

$$4\Phi(\zeta)=P+Q+O(|\zeta|^{-2}),\ \ 2\Psi(\zeta)=Q-P+O(|\zeta|^{-2}), \quad |\zeta|\to\infty. \tag{17}$$

For a circular integration path, substitution of the convergent Laurent expansions

$$\omega(\zeta)=\zeta+\sum_{k=1}^{\infty}d_k\zeta^{-k},\ \ \Phi(\zeta)=\frac{P+Q}{4}+\sum_{k=2}^{\infty}a_k\zeta^{-k}, \qquad \zeta\in\Sigma_2+\gamma \tag{18}$$

transforms (16a), with the use of (2), into a more easily handled infinite system of linear algebraic equations in $\{a_k\}$, $k\geq 2$:

$$\begin{gathered}-\lambda a_{m+2}+\lambda\sum_{k=2}^{m}(m-k+1)\bar{d}_{m-k+1}a_k-(m+1)\sum_{k=2}^{\infty}\bar{d}_{m+k+1}\bar{a}_k=A_m,\\ m=0,1,\ldots,\ \ A_0=P,\ A_1=0,\ 2A_m=-(P+Q)(m+1)\bar{d}_{m+1},\ m\geq 2.\end{gathered} \tag{19}$$

In conformity with the asymptotics (17) we have $a_1=0$, so the first sum is omitted in (19) when $m=0, 1$.

At $\lambda=-1$, Equations (19) again go over to the resolving system for a traction-free circular hole derived by [Kalandia 1975] and extensively used in [Vigdergauz 2006].

Finally, with pure shear

$$Q=-P=1, \qquad \Phi(\zeta)=O(|\zeta|^{-2}), \tag{20}$$

the normalized energy increment possesses the form (see for instance [Jasiuk 1995])

$$\delta W(\Gamma)=4\pi f_1^{-1}a_2, \qquad Q=-P=1, \tag{21}$$

while all but the first equation in (19) become homogeneous:

$$A_0=1,\ \ A_m=0 \text{ for } m>0. \tag{22}$$

This completes the one-potential formulation (19) of the forward problem of finding the criteria (15b), (21) for inclusion shape Γ as given by the mapping function (18). Concluding this section, we note that the energy criterion (21) is computationally much simpler then $\mathcal{M}$, since it involves only the first Laurent term a_2. In the current context, the δW value is a byproduct of the direct problem solution for σ_M. For this reason, the δW-optimization is further addressed as a problem accompanying the $\mathcal{M}$-shape optimization.

3. Analytical truncation of the forward problem

In numerical applications, the infinite system (19) has to be truncated in some way. This is usually done by keeping only the first N equations, that is, by dropping high-order expansion terms both in $\omega(\zeta)$, so that

$$\omega(\zeta) = \zeta + \sum_{k=1}^{N} d_k \zeta^{-k} \qquad (d_k = 0 \ \text{ for } k > N), \tag{23}$$

and in $\Phi(\zeta)$, so that

$$\Phi(\zeta) = \sum_{k=2}^{N} a_k \zeta^{-k}, \qquad (a_k = 0 \ \text{ for } k > N); \tag{24}$$

see [Jasiuk 1995; Cherkaev et al. 1998] and [Tsukrov and Novak 2004], where the resolving system for $\Phi(\zeta)$ is derived by collocating the contact conditions at a finite number of points along the interface.

The N-term solution so obtained amounts to a finite approximation in inverse powers for the potential $\Phi(\zeta)$. This algorithm solves well the energy criterion (21) but it is too time-consuming for finding the boundary stresses (13), (14). Indeed, due to their local nature, double truncation (DT) requires a rather large value of N; otherwise spurious oscillations are produced along the interface, as exemplified in [Vigdergauz 2006]. As a remedy, we use here the specific structure of Equations (19) to restrict the truncations only to (23), while keeping all the coefficients a_k, $k = 2, 3, \ldots$, as in (18). This *single truncation* (ST) scheme allows us to perform this infinite sum *analytically* for any finite-term expansion of the mapping function $\omega(\zeta)$, and so yields a *finite* semianalytic approach for solving the *infinite* system (19). The ST scheme was proposed and detailed for a free-traction hole in [Vigdergauz 2006]. For reference, we go over it briefly, focusing on the differences between the earlier case and the one discussed here.

To begin with, the coefficients $\{d_m\}$ obey the necessary conditions of mapping univalency, namely

$$-\frac{1}{\sqrt{m}} \le d_m \le \frac{1}{\sqrt{m}}, \qquad m = 1, 2, \ldots, \tag{25}$$

following from the nonnegativeness of the area f_1 inside Γ [Schinzinger and Laura 1991]:

$$f_1 = \pi \left(1 - \sum_{k=1}^{\infty} k |d_k|^2 \right) \ge 0.$$

Though the asymptotics for the interval width is only $m^{-1/2}$ as $m \to \infty$, the coefficients $\{d_m\}$ actually tend to zero much faster, at least as fast as m^{-2}, provided Γ is a continuous curve [Schinzinger and Laura 1991]. It is precisely this asymptotic behavior that makes the assumed mapping truncation (23) numerically reasonable.

With the truncation (23), the second sum in (19) is also finite. It contributes to the first $N-2-m$ unknown entries $a_2, \ldots, a_{N-1-m}$ in the m-th equation, where $m < N-2$, and hence disappears in all equations from $m = N-2$ onward. As a result, each matrix row contains either N (at $m < N$) or $N+1$ (at $m = N, N+1, \ldots$) nonzero entries arranged as shown schematically on the next page for for $N = 3$ and the shear-type right-hand side (22).

$$\begin{Bmatrix} \times & \times & \times & & & \\ \times & \times & \times & & & \\ \times & \times & \times & & & \\ \times & \times & \times & \times & & \\ & \times & \times & \times & \times & \\ & & \times & \times & \times & \times \\ & & & \cdots & \cdots & \end{Bmatrix} \begin{Bmatrix} a_2 \\ a_3 \\ a_4 \\ a_5 \\ a_6 \\ a_7 \\ \cdots \end{Bmatrix} = \begin{Bmatrix} 1 \\ 0 \\ 0 \\ 0 \\ 0 \\ 0 \\ \cdots \end{Bmatrix} \tag{26}$$

Put differently, the finite expansion (23) decomposes the initial system (19) into two subsystems. The first is just the DT-reduced $N \times N$ nonhomogeneous system to solve the first N coefficients a_k, for $k = 2, 3, \ldots, N+1$. The second ST-specific homogeneous subsystem in the rest of unknowns a_k, $k > N+1$, is neglected in the DT-scheme. An important point is that its $(N+1)$-width band matrix comprises an infinite linear system of finite differences [Levy and Lessman 1959]

$$a_{m+2} - \sum_{k=1}^{N} k d_k a_{m-k+1} = 0, \qquad m = N,\ N+1, \ldots, \tag{27}$$

with constant coefficients $1, 0, -d_1, -2d_2, \ldots, -Nd_N$, which define the N-term Laurent expansion of $\omega'(\zeta)$, as seen from (23). In contrast to the first subsystem, these equations are free of the matrix parameter λ.

Solving (27) by a standard finite-differences approach [Levy and Lessman 1959] we obtain $\Phi(\zeta)$ after some algebra as a simple rational function of ζ^{-1}:

$$\Phi(\zeta) = \frac{R_N(\zeta^{-1})}{\zeta \omega'(\zeta)} \tag{28}$$

Here $R_N(\zeta)$ is a degree-N polynomial in ζ with coefficients linearly composed of the first $\{d_k\}$, $k \le N$:

$$R_N(\zeta) = \sum_{k=1}^{N} r_k \zeta^k, \quad \text{with } r_1 = a_2, \quad r_m = a_{m+1} + \sum_{j=1}^{m-1} (-1)^{m-j} (m-j+1) d_{m-j+1} a_j \text{ for } m \ge 2, \tag{29}$$

which in turn are to be solved for from the first $N \times N$ subsystem. In passing we note that $r_0 = 0$ to match the shear-type asymptotics (20).

The proposed algorithm works faster than its basic counterpart [Muskhelishvili 1975], which requires a time-consuming precomputation of the N-term expansion of the composed function $\omega(\zeta)/\overline{\omega'(1/\zeta)}$. This is of particular value when the same forward problem is repeatedly solved many times in evolutionary optimization methods.

The truncation (23) and the resulting finite expressions (28)–(29) allow us at last to reformulate the optimization problem in a numerically tractable form.

For a given finite number N of mapping coefficients and pure shear field $B = 0$, find the $\mathcal{M}$-optimal rigid inclusion shape on which

$$\mathcal{M} \equiv \max_{t \in \Gamma_N} \sigma_M(t) \equiv \max_{0 \le \theta \le 2\pi} \sigma_M(\xi \equiv \exp i\theta) \xrightarrow[\{\Gamma_N\}]{} \min, \tag{30}$$

where $\{\Gamma_N\}$ *denotes the set of all curves mapped onto the unit circle by* $\omega(\zeta)$ *with any admissible finite set* $\{d_m, m = \overline{1, N}\}$, *and* $d_m = 0, m > N$.

The accompanying δW-optimization problem is posed similarly.

4. One-term analytical relations at a rigid interface

It is well known that even a one-term conformal mapping covers a wide variety shape geometries: from a rectilinear cut (with the Zhukovsky function $\omega(\zeta) = \zeta + \zeta^{-1}$ — see [Schinzinger and Laura 1991]) to a $(p+1)$-cusped hypocycloid (with $\omega(\zeta) = \zeta + p^{-1}\zeta^{-p}$, $p = 2, 3, \dots$). With this in view, the one-term closed expressions for δW and σ_M are derived and analyzed below to gain qualitative insight into the optimal solution, which appears to depend on the rotational symmetry of the contour sought. This symmetry is defined through an integer parameter $p = 1, 2, \dots$, defined so that $\alpha = 2\pi/(p+1)$ is the minimal rotation angle transforming the contour to itself:

$$\omega(e^{i\alpha}\zeta) = e^{i\alpha}\omega(\zeta),$$

or, equivalently,

$$\omega(\zeta) = \zeta + \sum_{k=1}^{\infty} d_{pk}\zeta^{-pk}.$$

In particular, the one-term mapping takes the form

$$\omega(\zeta) = \zeta + d_p\zeta^{-p}, \quad \omega'(\zeta) = 1 - pd_p\zeta^{-p-1}, \quad f_1 = \pi(1 - pd_p^2), \tag{31}$$

and hence the summation coefficients in (29) simplify: $r_m = a_{m+1},\ m \geq 1$. As in the hole case [Vigdergauz 2006], this results in

$$\Phi(\zeta) = \frac{a_2\zeta^{p-1} + a_{p-1}\zeta^2}{\zeta^{p+1} - pd_p}, \tag{32a}$$

$$\sigma_M(\theta) = D_1(\lambda)F_1(\theta) + D_2(\lambda)F_2(\theta), \tag{32b}$$

$$F_1(\theta) = \left(\frac{a_2(\cos 2\theta - pd_p\cos(p-1)\theta) + a_{p-1}(\cos(p-1)\theta - pd_p\cos 2\theta)}{1 - 2pd_p\cos(p+1)\theta + p^2d_p^2}\right)^2, \tag{32c}$$

$$F_2(\theta) = \left(\frac{a_2(\sin 2\theta + pd_p\sin(p-1)\theta) + a_{p-1}(\sin(p-1)\theta + pd_p\sin 2\theta)}{1 - 2pd_p\cos(p+1)\theta + p^2d_p^2}\right)^2, \tag{32d}$$

where the dependence on λ is hidden in the Laurent coefficients a_2, a_{p-1} of the potential $\Phi(\zeta)$. They are found by solving the first nonvanishing equations (19). For $p \leq 3$, the second term a_{p-1} is zero and should be dropped from (31). The one-term results so obtained are detailed below for different symmetries. For convenience, the criteria are henceforth normalized to the interval [0, 1] by their counterparts $\delta W_0, \mathcal{M}_0$ for a circular inclusion, when $\gamma \equiv \Gamma$, $\omega(\zeta) = \zeta$, $f_1 = \pi$, $\Phi(\zeta) = -1/\lambda\zeta^2$ [Muskhelishvili 1975] and hence, with (21), (15),

$$\delta W_0 = -4/\lambda, \quad \sigma_M^2(\theta) = D_1(\lambda)\cos^2 2\theta + D_2(\lambda)^2\sin^2 2\theta, \tag{33a}$$

$$\mathcal{M}_0 = \max_\theta \sigma_M(\theta) = \sigma_M(\pi/4) = D_2^{1/2}(\lambda)/\lambda = (\lambda+1)\sqrt{3}/\lambda, \quad 1 \leq \lambda \leq 3. \tag{33b}$$

To avoid confusion, we note that the Dundurs correspondence ($\lambda = -1$, a traction-free circular hole under shear) does not hold for (33b). Here,

$$\max \sigma_M(\theta) = \sigma_M(0) = D_1^{1/2}(-1) = 2,$$
$$\min \sigma_M(\theta) = \sigma_M(\pi/4) = D_2^{1/2}(-1) = 0.$$

4.1. ***Twofold*** **($p = 1$)** ***and triangular symmetry*** **($p = 2$).** Here

$$a_2 = -\frac{1}{\lambda}, \quad \delta W_2 = -\frac{1}{1-2d_2^2}: \qquad d_p^{(\min)} = 0, \quad \min_{d_p} \delta W_p = 1. \tag{34}$$

A simple numerical check of (32b) in the univalency interval (25) shows further that $\min_{d_p} \mathcal{M} = 1$ at $d_p = 0$, independently of λ.

4.2. ***Square symmetry*** **($p = 3$).** Here

$$\begin{aligned} &a_2 = -\frac{1}{\lambda+d_3}, \quad \delta W_3 = \frac{\lambda}{(\lambda+d_3)(1-3d_3^2)}, \quad |d_3| \le \frac{1}{\sqrt{3}}, \\ &d_3^{(\min)} = \frac{\sqrt{\lambda^2+1}-\lambda}{3}; \quad \min_{d_3} \delta W_3 = \frac{9\lambda}{2(2\lambda+\sqrt{\lambda^2+1})(1-\lambda^2+\lambda\sqrt{\lambda^2+1})}. \end{aligned} \tag{35}$$

In contrast to the case (34), the square symmetric δW-optimal inclusion differs from a circle. It is shaped as a rounded square rotated by 45 degrees with respect to the axes X, Y. The roundness depends on λ and is measured by the deviation of $d_3^{(\min)}$ from the first mapping coefficient $d_3^{(\text{square})} = 1/6$ [Jasiuk 1995] of an exact square shape. It varies from ≈ 0.0286 at $\lambda = 1$ to ≈ 0.1126 at $\lambda = 3$. As a result, the energy $\delta W_3^{(\text{square})}$ exceeds the minimum (35) by ≈ 0.00308 at $\lambda = 1$ ($\min \delta W_3 \approx 0.93198$, $\delta W_3^{(\text{square})} \approx 0.93506$) and by ≈ 0.04251 at $\lambda = 3$ ($\min \delta W_3 \approx 0.99099$, $\delta W_3^{(\text{square})} \approx 1.03349$). The latter comparison shows that just small local improvements of an exact square shape near the angular points allow one to go beyond the circle-related value $\delta W^{(circle)} = 1$. This is also true for the multiterm approximation (Section 6) with $\delta W^{(\text{square})} = 1$ at $\lambda \approx 1.88149$.

Another observation shows that at $\lambda = 1$ (an incompressible matrix) the optimal coefficient $d_3^{(\min)} = (\sqrt{2}-1)/3$ is equal in value but opposite in sign to its counterpart for a hole under shear [Cherkaev et al. 1998; Vigdergauz 2006]. In other words, both one-term shapes are the same, differing only in orientation about the axes.

Similarly, the $\mathcal{M}$-optimal shape is also a rotated rounded square though with somewhat different value of the mapping coefficient.

The already noted resemblance of the energy optimal hole and the rigid inclusion at $\lambda = 1$ is of general nature and holds for any pair of mutually rotated square-symmetric shapes. Indeed, the mapping function

$$\omega(e^{i\frac{\pi}{4}}\zeta) = e^{\frac{\pi}{4}}\zeta + \sum_{k=1}^{\infty} e^{(1-4k)\frac{\pi}{4}} \frac{d_{4k-1}}{\zeta^{4k-1}} = e^{i\frac{\pi}{4}}\left(\zeta + \sum_{k=1}^{\infty}(-1)^k \frac{d_{4k-1}}{\zeta^{4k-1}}\right), \tag{36}$$

with alternating signs of the Laurent coefficients rotates a shape by 45 degrees. Substitution of (36) into the system (19) while putting $\lambda = -1$ results in a system equivalent to the traction-free hole conditions

(12), whose solution evidently takes the form

$$a_{4k-2}^{(hole)} = (-1)^k a_{4k-2}^{(\lambda=1)}; \qquad k = 1, 2, \ldots.$$

In particular $a_2^{(\text{hole})} = -a_2^{(\lambda=1)}$ and hence both (no normalized) energy increments are the same up to the sign.

4.3. *Higher symmetry* ($p \geq 4$).

$$a_2 = -\frac{\lambda}{\lambda^2 - (p-2)d_p^2}, \quad a_{p-1} = \frac{(p-2)d_p}{\lambda^2 - (p-2)d_p^2}, \qquad |d_p| \leq \frac{1}{\sqrt{p}},$$

$$\delta W_p = \frac{\lambda^2}{(\lambda^2 - (p-2)d_p^2)(1 - pd_p^2)}, \quad \min_{d_p} \delta W_p = 1, \quad d_p^{(\min)} = 0.$$

Again, as in Section 4.1, $\mathcal{M}$-optimal contour appears to be a circle with $\mathcal{M} = 1$.

The one-term results suggest that the most promising for further analysis is the fourfold ($p = 3$) symmetry case when the δW- and $\mathcal{M}$-optima are achieved at similarly rotated square-like shapes. As numerically shown in Section 6, this pattern is preserved for multiterm $N > p = 3$ approximations.

5. The GA scheme

As described above, the shape optimization problem is solved by minimizing either $\mathcal{M}$ or δW criterion over a N-parameter set of closed curves. In principle, the single truncation approach (27)–(29) explicitly provides all the information required by a standard gradient-based optimization. However, this results in too complicated analytical manipulations and time-consuming calculations. A good alternative is a relatively novel genetic algorithm, which mimics the Darwinian evolution paradigm, both in the concept and in the terms. Devised by Holland [1975], the GA finds wide application in engineering. In the current context, the relevant information is detailed in [Vigdergauz 2006], where a fairly standard GA is applied to find the stress-minimizing hole under remote shear.

The GA optimization process is governed by a number of parameters that control its performance. Here parameter tuning is of lesser importance due to the relatively small problem size (the first five nonzero mapping terms appear to provide a good convergence in the square symmetric case). For this reason, we use the parameter values found in the process of hole shape optimization [Vigdergauz 2006].

6. Multiterm numerical results

In quantifying the shape optimization effect on the matrix stress-strain state, we first find a compromise truncation number N to achieve a reasonable numerical accuracy at a not-too-large computational cost. Tables 1 and 2 display the optimization results obtained by sequentially truncating the resolving system (19) at the first nonvanishing equation in the square symmetric case.

The observed fast convergence is explained differently for either criterion. As noted in Section 2, the higher mapping coefficients go to zero rather rapidly and hence have little or no effect on the integral-type energy increment δW. On the other hand, they are responsible for forming large curvature isolated shape points (see Figure 2) which may only worsen the local criterion $\mathcal{M}$. In this respect, of special interest is the von Mises stress distribution along the $\mathcal{M}$-optimal interface as depicted in Figure 3 in dependence of

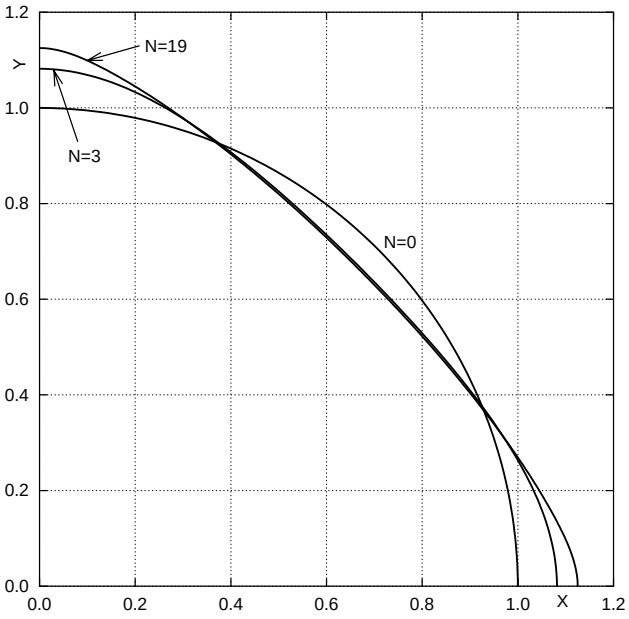

Figure 2. A quarter of the M-optimal rigid inclusion under simple shear for different number of the first mapping terms.

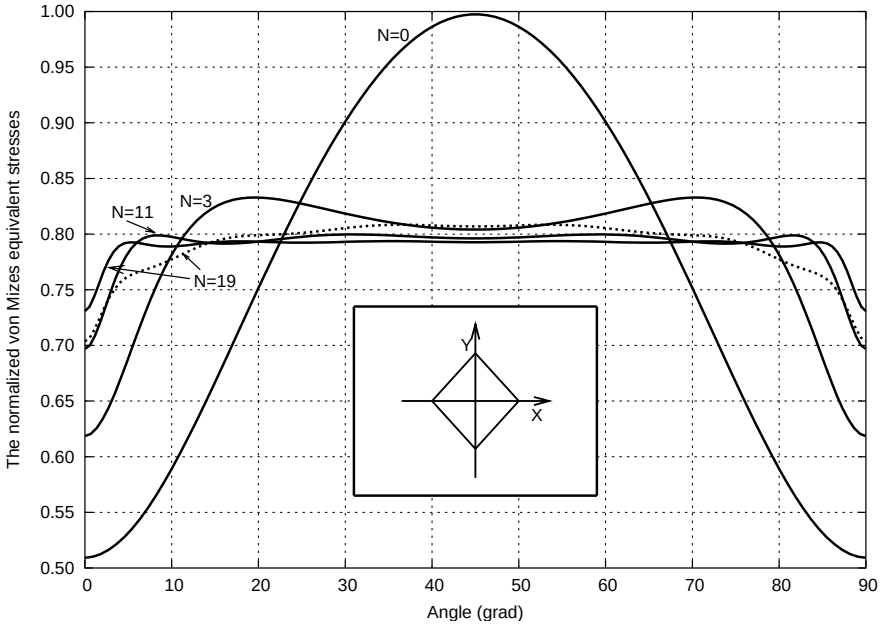

Figure 3. Distribution of the normalized von Mises equivalent stresses along the square-like M-optimal rigid inclusion in dependence of the problem mapping size beginning with a circle ($N = 0$). The δW-optimal distribution (dotted) is also added for comparison. The inset shows the inclusion orientation.

N	d_3	d_7	d_{11}	d_{15}	d_{19}	$\delta W_{\min}$	$\delta W^{(\text{square})}$
3	0.078689					0.980356	1.006993
7	0.080125	0.006922				0.979970	1.005677
11	0.080356	0.007244	0.001794			0.979929	1.005269
15	0.080415	0.007319	0.001910	0.000671		0.979921	1.005102
19	0.080434	0.007342	0.001942	0.000722	0.000303	0.979919	1.005083

Table 1. A rigid square symmetric inclusion under remote shear at $\lambda = 2$: the global minimum $\delta W_{\min}$ and its mapping coefficients for the first values of N. The energy values for an exact square shape are also added for comparison.

N. The curves are seen to converge to the uniform distribution, with successively diminishing deviations occurring near the angles $\theta_l = l\pi/2, l = 0, 1, \ldots$ In some contrast, the δW-optimal von Mises stresses (the dotted line) show diminishing local peaks, though generally this is a very similar pattern. The same situation is numerically observed everywhere in the interval $1 \le \lambda \le 3$. This allows us to conservatively conclude that *the full-size optimal solution should led to to the exactly uniform distribution of the von Mises stresses along the rigid inclusion shape with their level depending on* λ.

Of course, it is only a numerical conjecture rather than a rigorous analytical proof which is outside of our current scope.

The rest of the numerical results is obtained by holding the first five terms $d = 4_{4k-1}, k = 1, \ldots, 5$, or, equivalently by truncating the system at $N = 19$.

Figure 4 exemplifies the von Mises stress levels around the $\mathcal{M}$-optimal inclusion at $\nu_{\text{stress}} = 1/3$, $(\lambda = 2)$. As one might expect, the maximum stress gradient occurs near the angles θ_l where the level lines thicken.

Figure 5 displays the $\mathcal{M}$- and δW-optimal shapes for the limiting values of λ. The δW-optimal shapes, as compared to their $\mathcal{M}$-optimal counterparts, have angular points. Though distinct, they do not reach the critical openings $\alpha(\lambda)$ where the stresses become singular, contrary to a physical possibility for real material.

N	d_3	d_7	d_{11}	d_{15}	d_{19}	$\mathcal{K}_{\min}$	δW
3	0.067933					0.834158	0.980727
7	0.007981	0.005158				0.808959	0.979996
11	0.084671	0.006868	0.001245			0.800220	0.979997
15	0.086647	0.007422	0.001631	0.000394		0.796231	0.980050
19	0.088398	0.008069	0.002011	0.000642	0.000194	0.793977	0.980122

Table 2. A rigid square symmetric inclusion under remote shear at $\lambda = 2$: the conformal mapping coefficients and the local criterion $\mathcal{K}_{\min}$ resulted from the GA optimization process for different values of N. The corresponding global criterion δW is also shown, for comparison with its optimal values in Table 1.

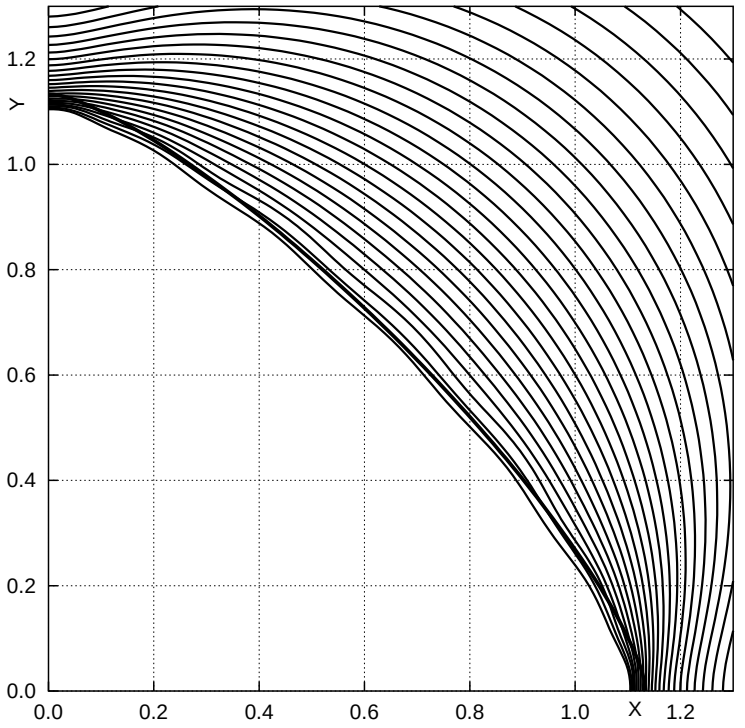

Figure 4. A quarter of the $\mathcal{M}$-optimal rigid inclusion under simple shear: von Mises equivalent stress contours at $\lambda = 2$.

The formation of the angles is comprehensively analyzed by [Cherkaev et al. 1998]. Here we only note that $\alpha(\lambda)$ are in the numerically found interval

$$\alpha(1) \le \alpha(\lambda) \le \alpha(3), \qquad \alpha(1) \approx 102.5^\circ, \quad \alpha(3) \approx 152.5^\circ.$$

Another observation is that the δW-optimal shape is flatter than its $\mathcal{M}$-optimal counterpart at $\lambda = 1$ and quite the reverse at $\lambda = 3$. This suggest that there is an intermediate value λ^* at which the shapes and their criteria come the closest together. The computation gives $\lambda^* \approx 1.712\ldots$.

Finally, Figure 6 gives the criteria at hand for either of the two optimal shapes in dependence of λ. It is seen that the δW-criterion of the $\mathcal{M}$-optimal shapes markedly exceeds $\min \delta W$ only near the point $\lambda = 1$. Contrastingly, the $\mathcal{M}$-criterion of the δW-optimal shapes is substantially above its minimum everywhere except near the above-found point λ^*. Put it differently, the δW-optimization is performed partly at the penalty of increasing the $\mathcal{M}$-criterion

7. Conclusions and future applications

We have presented a novel semianalytical solution for isolated, nondeformable inclusion subjected to pure remote shear. An inclusion shape is presented as a finite-term conformal map of a circle rather than by more traditional nodal points. This allows to pose the optimization as a small-size numerical problem with linear constraints particularly amenable to the GA search. Another essential idea is to express the

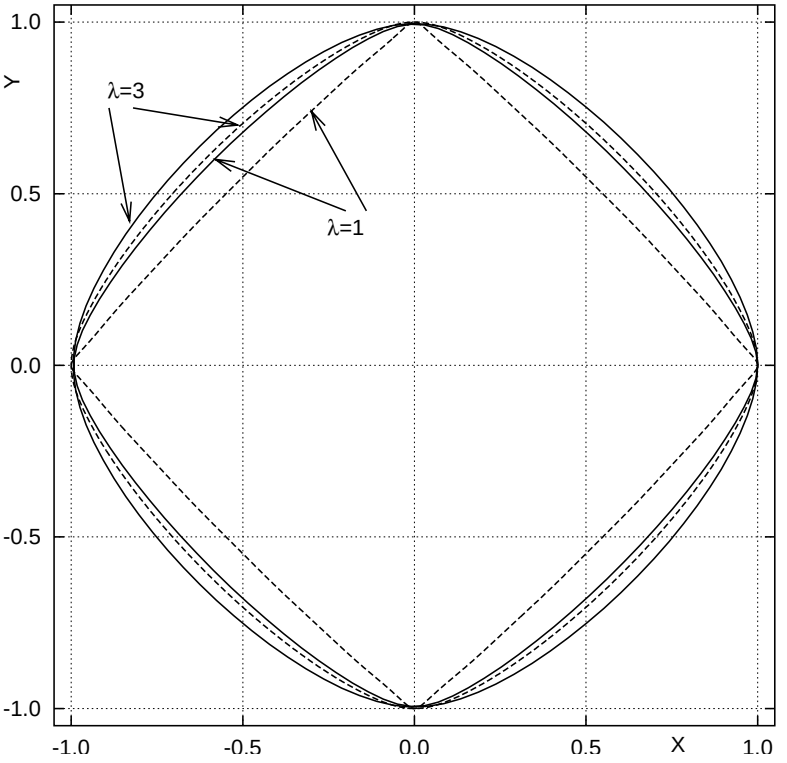

Figure 5. The $\mathcal{M}$-optimal and δW-optimal (dotted) inclusion shapes for the limiting values of the elastic parameters λ.

stresses through only one KM potential whose infinite Laurent tail is summed in a closed form. The numerical accuracy so achieved permits to solves the yet unconsidered problem of globally minimizing the von Mises local criterion over a broad range of continuous curves. The results obtained are in strong parallel to those for the optimal hole [Vigdergauz 2006]:

• The both shapes differ from a circle only in the square symmetric case when they are close to a slightly rounded square located in a specifically rotated position relative to each other;

• For the δW-criterion the roundness is combined with four distinct angular points whose opening is greater than the critical values which bring stress singularities;

• The δW- and $\mathcal{M}$-optimal shapes are very similar though not exactly the same;

• Under the $\mathcal{M}$-criteria, the von Mises stress distribution becomes uniform along the optimal interfaces.

Of course, these conclusions are arrived at only numerically and the analytical proof would be very desirable.

It is worthy of note that the conformal mapping is used not only for the shape description but also to transform the stress field around the shape. This may be done only for a hole or a rigid inclusion which exhaust the setup with a single deformable region. In order to fill gap between these limiting cases, an optimal shaping of elastic inclusion should be considered. This problem is far too complicated

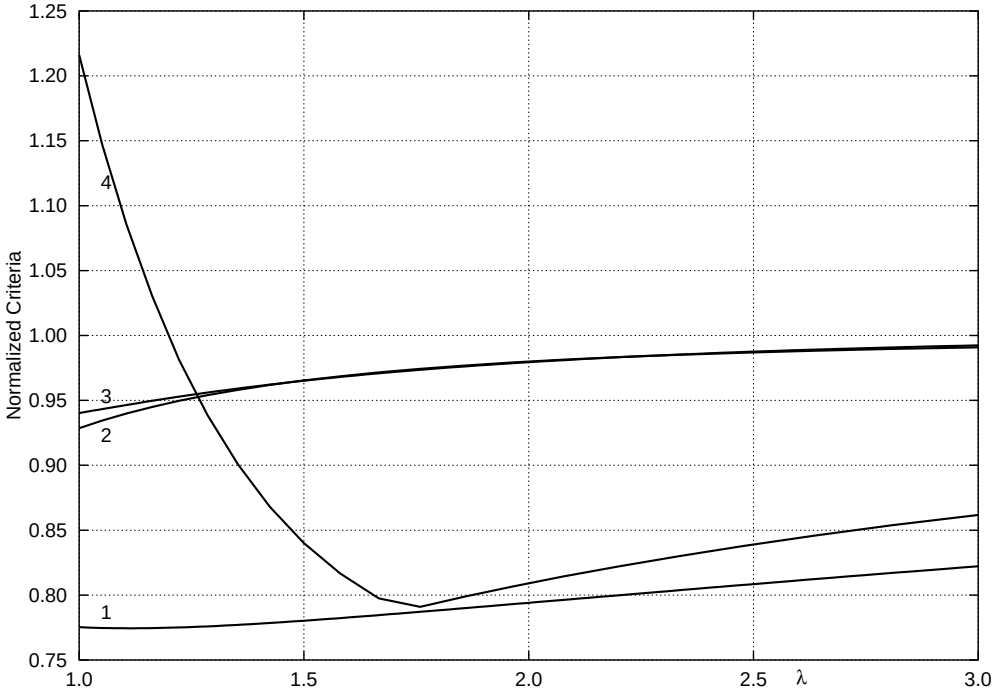

Figure 6. $\min \mathcal{M}$ (curve 1), $\min \delta W$ (curve 2), δW of $\mathcal{M}$-optimal shapes (curve 3), $\mathcal{M}$ of δW-optimal shapes (curve 4) as functions of λ.

because both elastic regions may not be mapped simultaneously. Nevertheless, the proposed mapping parameterization inside the GA seems to be potentially useful here too.

References

[Cherepanov 1974] G. P. Cherepanov, "Inverse problem of the plane theory of elasticity", *Prik. Mat. Mekh.* **38**:6 (1974), 963–979. In Russian; translated in *J. Appl. Math. Mech.* **38**:6 (1974), 915–931.

[Cherepanov 1997] G. P. Cherepanov, *Methods of fracture mechanics: Solid matter physics*, Solid Mechanics and its Applications **51**, Kluwer, Boston, 1997.

[Cherkaev et al. 1998] A. V. Cherkaev, Y. Grabovsky, A. B. Movchan, and S. K. Serkov, "The cavity of the optimal shape under the shear stresses", *Int. J. Solids Struct.* **35**:33 (1998), 4391–4410.

[England 1971] A. H. England, *Complex variable methods in elasticity*, Wiley, London, 1971. Reprinted Dover, New York, 203.

[Gen and Cheng 1997] M. Gen and R. Cheng, *Generic algorithm and engineering design*, Wiley, New York, 1997.

[Grabovsky and Kohn 1994] Y. Grabovsky and R. V. Kohn, "Microstructures minimizing the energy of a two phase elastic composite in two space dimensions, II: The Vigdergauz microstructure", *J. Mech. Phys. Solids* **43** (1994), 949–972.

[Holland 1975] J. H. Holland, *Adaptation in natural and artificial systems*, University of Michigan Press, Ann Arbor, 1975.

[Jasiuk 1995] I. Jasiuk, "Cavities *vis-a-vis* rigid inclusions: Elastic moduli of materials with polygonal inclusions", *Int. J. Solids Struct.* **32**:3-4 (1995), 407–422.

[Kalandia 1975] A. I. Kalandia, *Mathematical methods of two-dimensional elasticity*, Mir, Moscow, 1975.

[Levy and Lessman 1959] H. Levy and F. Lessman, *Finite difference equations*, Pitman, London, 1959. Reprinted Dover, New York, 1992.

[Muskhelishvili 1975] N. I. Muskhelishvili, *Some basic problems of the mathematical theory of elasticity*, 2nd ed., Noordhoff, Leiden, 1975.

[Osyczka 2001] A. Osyczka, *Evolutionary algorithms for single and multicriteria design optimization*, Springer Physica-Verlag, Heldelberg, 2001.

[Savin 1961] G. N. Savin, *Stress concentration around holes*, Pergamon, New York, 1961.

[Schinzinger and Laura 1991] R. Schinzinger and P. A. A. Laura, *Conformal mapping: methods and applications*, Elsevier, New York, 1991. Reprinted Dover, New York, 2003.

[Tsukrov and Novak 2004] I. Tsukrov and J. Novak, "Effective elastic properties of solids with two-dimensional inclusions of irregular shapes", *Int. J. Solids Struct.* **41**:24-25 (2004), 6905–6924.

[Vigdergauz 1976] S. B. Vigdergauz, "Integral equation of the inverse problem of the plane theory of elasticity", *Prik. Mat. Mekh.* **40**:3 (1976), 566–569. In Russian; translated in *J. Appl. Math. Mech.* **40**:3 (1976), 518–522.

[Vigdergauz 2006] S. Vigdergauz, "The stress-minimizing hole in an elastic plate under remote shear", *J. Mech. Mater. Struct.* **1**:2 (2006), 387–406.

Received 24 Jul 2006. Accepted 9 Oct 2006.

SHMUEL VIGDERGAUZ: smuel@iec.co.il
Research and Development Division, The Israel Electric Corporation Ltd., P.O.Box 10, Haifa 31000, Israel